Monthly Notices
of the
ROYAL ASTRONOMICAL SOCIETY

Mon. Not. R. Astron. Soc. **416,** 2078–2089 (2011) doi:10.1111/j.1365-2966.2011.19183.x

GRB 090618: detection of thermal X-ray emission from a bright gamma-ray burst

K. L. Page,[1⋆] R. L. C. Starling,[1] G. Fitzpatrick,[2] S. B. Pandey,[3,4] J. P. Osborne,[1] P. Schady,[5] S. McBreen,[2] S. Campana,[6] T. N. Ukwatta,[7] C. Pagani,[1] A. P. Beardmore[1] and P. A. Evans[1]

[1]*Department of Physics & Astronomy, University of Leicester, University Road, Leicester LE1 7RH*
[2]*School of Physics, University College, Dublin, Belfield, Stillorgan Road, Dublin 4, Ireland*
[3]*Randall Laboratory of Physics, University of Michigan, 450 Church Street, Ann Arbor, MI 48109-1040, USA*
[4]*Aryabhatta Research Institute of Observational Sciences, Manora Peak, Nainital 263129, India*
[5]*Max-Planck-Institut für extraterrestrische Physik, Giessenbachstraße 1, 85748 Garching, Germany*
[6]*INAF - Osservatorio Astronomico di Brera, Via Bianchi 46, I-23807 Merate (Lc), Italy*
[7]*Department of Physics and Astronomy, Michigan State University, East Lansing, MI 48824, USA*

Accepted 2011 June 2. Received 2011 June 1; in original form 2011 April 15

ABSTRACT

GRB 090618 was an extremely bright burst, detected across the electromagnetic spectrum. It has a redshift of 0.54 and a supernova (SN) was identified in ground-based photometry. We present a thorough analysis of the prompt and early afterglow emission using data from *Swift*, *Fermi* Gamma-ray Burst Monitor and *ROTSE*, in which we track the evolution of the synchrotron spectral peak during the prompt emission and through the steep decay phase. We find evidence of a thermal X-ray component alongside the expected non-thermal power-law continuum. Such a component is rare among gamma-ray bursts (GRBs), with firm data for only GRBs 060218 and 100316D so far, and could potentially originate from an SN shock breakout, although there remains doubt regarding this explanation for any of the bursts. However, in contrast to these other *Swift* GRB–SNe with similar thermal signatures, GRB 090618 is a much more 'typical' burst: GRB–SNe 060218 and 100316D were both low-luminosity events, with long durations and low peak energies, while GRB 090618 was more representative of the wider population of long GRBs in all of these areas. It has been argued, based both on theory and observations, that most long GRBs should be accompanied by SNe. If this thermal X-ray component is related to the SN, its detection in GRB 090618, a fairly typical burst in many ways, may prove an important development in the study of the GRB–SN connection.

Key words: gamma-ray burst: general – X-rays: individual: GRB 090618.

1 INTRODUCTION

Gamma-ray bursts (GRBs) are intrinsically luminous objects, allowing them to be detected right across the Universe, from relatively nearby locations [e.g. GRB 980425 at a redshift, z, of 0.0085 (Tinney et al. 1998) and GRB 060218 at $z = 0.0331$ (Campana et al. 2006)] out to great distances [e.g. GRB 090423 with $z = 8.2$ (Tanvir et al. 2009; Salvaterra et al. 2009) and GRB 090429B at $z = \sim 9.4$ (Cucchiara et al. 2011)]. While the very high-z objects allow us to probe the early Universe, learning more about the process of reionization, low-z objects provide a route to gathering more detailed information about their host galaxies, progenitors and environments.

That there is a connection between long GRBs (typically $T_{90} > 2$ s; Kouveliotou et al. 1993) and core-collapse supernovae (SNe) has been known since 1998, when GRB 980425 was identified with SN 1998bw (Galama et al. 1998), with GRB 030329 and SN 2003bh (e.g. Stanek et al. 2003; Willingale et al. 2004) providing further strong evidence; see Woosley & Bloom (2006) for a review of the SN-GRB connection. The relationship is not yet fully understood, however, since there are some nearby, long GRBs for which no SN has been detected [e.g. GRB 060614 (Della Valle et al. 2006; Fynbo et al. 2006; Mangano et al. 2007; Caito et al. 2009; Xu et al. 2009) and GRB 060505 (Fynbo et al. 2006; Ofek et al. 2007; Xu et al. 2009)]. A number of explanations have been suggested for these oddities, including that the apparently long burst could have been produced via a binary merger, through the explosion of a 'fall-back' SN if the star forms a non-rotating black hole or a 'dark hypernova' (Nomoto et al. 2004, 2007).

⋆E-mail: kpa@star.le.ac.uk

Since GRBs 980425 and 030329, there have been a number of other GRB–SNe associations spectroscopically confirmed, most recently GRB 101219B/SN 2010ma (Sparre et al. 2011), GRB 100316D/SN 2010bh (Starling et al. 2011) and GRB 060218/SN 2006aj (Campana et al. 2006), in addition to other GRBs which show the characteristic 'hump' of an SN in their optical photometry. GRB 090618 was an extremely bright burst (at all wavelengths) detected both by *Swift* and *Fermi*, at a redshift of 0.54 (Cenko et al. 2009; Fatkhullin et al. 2009). Cano et al. (2011) present optical data for this burst, revealing a probable SN-bump in the light curves, peaking a few tens of days after the GRB trigger. Very bright bursts such as GRB 090618 permit analysis of exceptional detail, helping to reveal the underlying physics of the processes involved. Previous examples of bright, well-observed bursts include GRB 030329 (also a GRB–SN; e.g. Stanek et al. 2003; Willingale et al. 2004), GRB 061121 (Page et al. 2007) and GRB 080319B (e.g. Racusin et al. 2008).

In Section 2 we present the γ-ray, X-ray, UV and optical observations, both spectral and temporal, while in Section 3, GRB 090618 is compared with other GRB–SNe. The results and conclusions are summarized in Section 4.

2 OBSERVATIONS

Swift (Gehrels et al. 2004), *Fermi*-GBM[1] (von Kienlin et al. 2004; Meegan et al. 2009), *AGILE*[2] (Tavani et al. 2009), *Konus* and the RT-2[3] Experiment (on-board the CORONAS-PHOTON[4] satellite) all triggered on GRB 090618 (Golenetskii et al. 2009; Longo et al. 2009; McBreen 2009; Schady et al. 2009b; Rao et al. 2009, 2011), which was also detected in γ-rays by the *Suzaku*-WAM[5] (Kono et al. 2009) and *INTEGRAL*-Spectrometer on Integral (SPI)-Anti-Coincidence Shield (ACS) (Beckmann, private communication). The *Swift*-BAT[6] (Barthelmy et al. 2005) trigger time was 08:28:29 UT on 2009 June 18 and this will be used as T_0 throughout the paper. The trigger times from the other satellites are a few seconds earlier: *Fermi*: 08:28:26.66 UT (McBreen 2009); *AGILE*-Mini-Calorimeter (MCAL) : 08:28:24.77 UT (Longo et al. 2009); *Konus*-Wind: 08:28:24.97 UT and *Konus*-RF : 08:28:27.06 UT (Golenetskii et al. 2009); *Suzaku*-WAM: 08:28:25.59 UT (Kono 2009; Kono et al. 2009).

As well as an extremely bright initial X-ray source (Beardmore & Schady 2009) detected by the *Swift*-XRT[7] (Burrows et al. 2005), the burst showed a bright optical afterglow which was seen by *Swift*-UVOT[8] (Roming et al. 2005; Schady 2009; Schady et al. 2009b), P60 (Cenko 2009), Katzman Automatic Imaging Telescope (KAIT) (Perley 2009), *ROTSE*-III[9] (Rujopakarn et al. 2009; the first image was collected a mere 6.7 s after the time of the GRB Coordinates Network (GCN) notice), the Observatorio Astrofisico Guillermo Haro (Carraminana, Alvarez Ochoa & Miramon 2009), FT-N[10] (Melandri et al. 2009), LOAO[11] (Im, Park & Urata 2009a), SARA[12] (Updike et al. 2009a,b), LT[13] (Cano et al. 2009), OAA[14] (Fernandez-Soto, Peris & Alonso-Lorite 2009), CrAO[15] (Rumyantsev & Pozanenko 2009), BOAO[16] (Im, Jeon & Urata 2009b), SAO RAS[17] (Fatkhullin et al. 2009), RTT150[18] (Galeev et al. 2009; Khamitov et al. 2009), PAIRITEL[19] (Morgan, Klein & Bloom 2009), HCT[20] (Anupama, Gurugubelli & Sahu 2009), Mondy (Klunko, Volnova & Pozanenko 2009) and the Lick Observatory. Using the Kast Spectrograph at the Lick Observatory, Cenko et al. (2009) determined the redshift of GRB 090618 to be 0.54; this was confirmed by Fatkhullin et al. (2009). A grism spectrum was also obtained by the UVOT, but the afterglow was too faint ($u \sim$14.6) to reveal any strong features.

In addition, a radio afterglow was detected by the AMI[21] Large Array (Pooley 2009a,b), the VLA[22] (Chandra & Frail 2009) and WSRT[23] (Kamble, van der Horst & Wijers 2009); see also Cano et al. (2011).

The *Swift* data in this paper have been processed using the standard procedures, but using a pre-release gain file for the XRT spectra which accounts for offsets caused by radiation-induced charge traps in the CCD detector. Corresponding pre-release (version 013) response matrix and ancillary response files were used for both the Windowed Timing (WT) and Photon Counting (PC) mode data.

The XRT light curve was obtained from the online repository (Evans et al. 2007, 2009) provided by the University of Leicester. The early WT data were heavily piled-up, so the central 94-arcsec (diameter) were excluded when creating the spectra and light curve for the piled-up portion (count rate $\gtrsim$100 count s^{-1}) of the observation. The first few snapshots of PC data also suffered from pile-up which was again accounted for by use of an annular extraction region, with an initial exclusion radius of 6 arcsec which was decreased as the count rate dropped. PC data with a count rate of $<$0.6 count s^{-1} were considered to be free from pile-up.

Throughout this paper, we adopt the convention of $F_{\nu,t} \propto \nu^{-\beta} t^{-\alpha}$ (photon spectral index $\Gamma = \beta + 1$), where $F_{\nu,t}$ is the flux density, ν is the observed frequency and t is the time since the onset of the burst. Errors are given at 90 per cent confidence unless otherwise stated.

2.1 γ-rays

GRB 090618 was strongly detected by the *Swift*-BAT (Schady et al. 2009b) and *Fermi*-GBM (McBreen 2009), and showed a bright, multipeaked structure, with $T_{90} \sim 113$ s (over 15–150 keV; measured from the BAT data). The source was 133° from the *Fermi*-LAT[24] boresight (McBreen 2009), so no useful LAT data were

[1] Gamma-Ray Burst Monitor
[2] *Astrorivelatore Gamma as Immagini ultra Leggero*
[3] Roentgen Telescope-2
[4] *Complex Orbital Observations Near-Earth of Activity of the Sun* satellite
[5] Wide-band All-sky Monitor
[6] Burst Alert Telescope
[7] X-ray Telescope
[8] UV/Optical telescope
[9] *Robotic Optical Transient Search Experiment*
[10] Faulkes Telescope North
[11] Mount Lemmon Optical Astronomy Observatory
[12] Southeastern Association for Research in Astronomy
[13] Liverpool Telescope
[14] Observatorio Astronomico de Aras
[15] Crimean Astrophysical Observatory
[16] Bohyunsan Optical Astronomical Observatory
[17] Special Astrophysical Observatory of the Russian Academy of Science Institution
[18] 150-cm Russian-Turkish Telescope
[19] Peters Automated Infrared Imaging Telescope
[20] Himalayan Chandra Telescope
[21] Arcminute Microkelvin Imager
[22] Very Large Array
[23] Westerbork Synthesis Radio Telescope
[24] Large Area Telescope

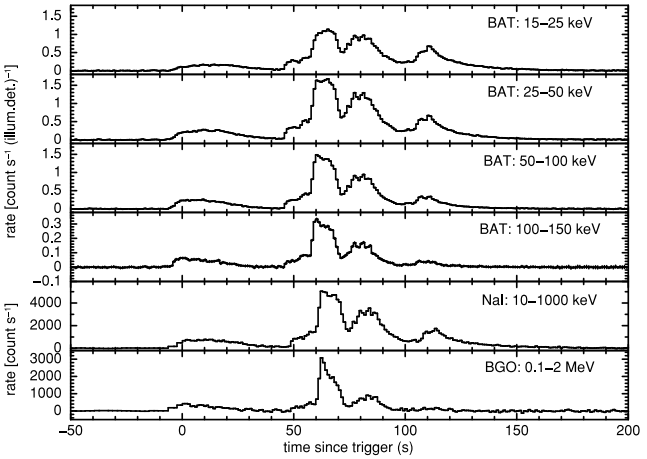

Figure 1. BAT and GBM (NaI and BGO) light curves of GRB 090618 over their standard energy bands, each showing strong peaks. There are far fewer counts above 100 keV in the BAT and so the ordinate for the 100–150 keV curve covers a much smaller range than for the lower energies.

obtained. The *Fermi*-GBM data were collected with the NaI-4 and Bismuth Germanate (BGO)-0 detectors (energy ranges of 8–1000 and 200–40 000 keV, respectively). Following an initial smooth peak lasting ∼50 s, there was a second episode of emission, consisting of three overlapping peaks (Baumgartner et al. 2009). The BAT and GBM light curves are shown in Fig. 1; note that the last peak (at ∼110 s) was barely visible in the highest energy (GBM-BGO) band.

Both the time-averaged (McBreen 2009; Sakamoto, Ukwatta & Barthelmy 2009) and time-sliced spectra (see below) are better fitted (>99.99 per cent confidence improvement in each case when compared to a simple power law) by a power law with exponential cut-off [$A(E) = KE^{-\Gamma}\mathrm{e}^{-E/E_{\rm cut}}$, where $E_{\rm cut}$ is the e-folding energy of the exponential cut-off and K is the normalization in units of photons keV^{-1} cm^{-2} s^{-1} at 1 keV]. A cut-off power law is used here as a simplification of the Band function (Band et al. 1993), since the higher energy index in the Band model cannot be well constrained in the BAT data alone, although the GBM data do help to constrain the fits over most of the time-slices. The typical high-energy index, β, for the spectral fits where the slope is constrained is −2.4. In the cut-off power-law model, $E_{\rm cut}$ is related to the peak energy, $E_{\rm peak}$, by $E_{\rm peak} = (2 - \Gamma) \times E_{\rm cut}$.

Simultaneous time-sliced spectra were extracted for both BAT and GBM data. Following Page et al. (2009b), the normalization offsets between BAT and the GBM-n4 and -b0 detectors were estimated: all 14 time-slices were fitted simultaneously in XSPEC (Arnaud 1996) with a cut-off power-law model, with the constant of normalization for the BAT set to unity, while the constants for the n4 spectra were all tied together (likewise for the b0 spectra) and allowed to vary with respect to the BAT; the other fit parameters were tied between BAT and GBM for each individual time-slice. This method gave a relative normalization of 1.29 for the n4 detector and 1.00 for b0, and provided a much better fit than forcing the n4 and b0 normalizations to be equal to each other ($\Delta\chi^2$ of 834). This factor between the NaI and BGO normalizations is very similar to that found by Ackermann et al. (2011), and was used in all subsequent spectral fitting. Similar results were also obtained using the *Fermi* software package RMFIT (Mallozzi, Preece & Briggs 2005).

$E_{\rm peak}$ initially decreases with time (Fig. 2), but moves to higher energies during the largest peak in the γ-ray emission, ∼60–70 s after the trigger, indicating that the spectrum is hardening during

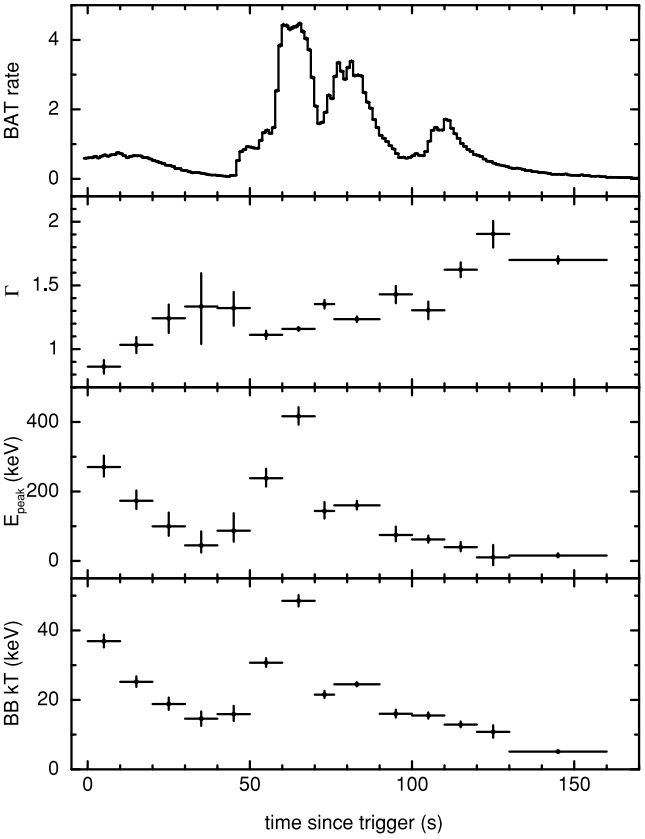

Figure 2. The variation of Γ, $E_{\rm peak}$ (both from the cut-off power-law model) and BB temperature from spectral fits to the BAT+GBM data; the final time-slice, from 130–160 s after the trigger, also includes XRT data. The BB temperature plotted for the final time-slice corresponds to the hotter of the two components discussed in the text. $E_{\rm peak}$ typically moves to lower energies, although there is a clear hardening (the peak of the spectrum moving to higher energies) during the largest flare in the γ-ray light curve (which is shown in the top panel).

the flares, as is typical (e.g. Golenetskii et al. 1983; Ford et al. 1995; Borgonovo & Ryde 2001; Goad et al. 2007; Page et al. 2007; Page et al. 2009b); the movement of the peak to higher energies during flaring activity has also been shown in *Swift* data by Butler & Kocevski (2007). In general, there is a positive trend between peak energy and γ-ray flux in our data. There are simultaneous XRT data for the final time-slice considered, between 130 and 160 s after the trigger, at which time $E_{\rm peak}$ is still above the XRT band, at 13 ± 3 keV.

A joint fit to the BAT, GBM-n4 and GBM-b0 spectra extracted over the BAT T_{90} interval (10–123 s after the trigger) gives $\Gamma = 1.35 \pm 0.02$ and $E_{\rm peak} = 211^{+22}_{-20}$ keV. This leads to a decrease of 2852 in χ^2 [for 1 degree of freedom (d.o.f.)] compared to a single power law, showing that the exponential cut-off is a vast improvement, as was the case for all the time-sliced spectra, too. Fitting the Band function in this case does actually lead to a further improvement in χ^2 of 246 for 1 d.o.f. (χ^2/d.o.f. = 930/298), with $\alpha = -1.09 \pm 0.04$, $\beta = -2.06 \pm 0.03$ and $E_{\rm peak} = 130^{+12}_{-11}$ keV, very similar to the parameters found by Bissaldi et al. (2011) for fitting the time-integrated GBM data (taken from a slightly different interval) alone. The cut-off power-law model leads to a fluence estimate of 2.2×10^{-4} erg cm^{-2} over 1 keV to 10 MeV in the rest frame (z = 0.54), corresponding to an isotropic energy release of 2.5×10^{53} erg. These values show GRB 090618 to be a typical burst in

the $E_{\rm peak}$–$E_{\rm iso}$ plane (Amati 2006). The burst is at the high-fluence end of the relation between the 11-hr X-ray afterglow flux density and the prompt fluence discussed by Gehrels et al. (2008).

An alternative to fitting the γ-ray spectrum with a cut-off power law is to use a combination of a power law and a thermal (blackbody) component, as discussed by Ryde (2004), Ryde & Pe'er (2009) and Guiriec et al. (2010); the blackbody (BB) then accounts for the curvature which is otherwise modelled by a break in the power law. It has been suggested that thermal components such as these could explain the hard early spectra which are inconsistent with synchrotron emission (Preece et al. 1998; Ghisellini, Celotti & Lazzati 2000; Savchenko & Neronov 2009). A component in addition to the Band function has also been identified in some *Fermi*-LAT spectra (e.g. GRB 090902B; Abdo et al. 2009), which could be modelled as high-temperature thermal emission (see also Ryde et al. 2010; Zhang et al. 2011b). Such a quasi-thermal model (power law plus BB) was applied to the GRB 090618 BAT+GBM data (see Section 2.2.1 for an investigation into possible thermal emission in the XRT data), finding generally acceptable results, although not as good (at >99.99 per cent confidence) as using a cut-off power law [similar to the fits by Page et al. (2009b) for GRB 080810]; the temperatures are included in the bottom panel of Fig. 2. The BB component accounts for the curvature of the spectrum in place of a cut-off in the power law, peaking in temperature at the time of the highest $E_{\rm peak}$ (during the brightest peak of the γ-ray light curve). This is not quite as described by Ryde (2004), where the observed temperature (after an initially constant value for the first 1–3 s) decreases as a power law in time; however, such characteristic cooling is shown for a single pulse, while the γ-ray light curve of GRB 090618 consists of a series over overlapping pulses which could hide the cooling behaviour.

The final time bin (130–160 s after the trigger) in Fig. 2 also included XRT data; as discussed in Section 2.2.1, the early X-ray data show evidence for a thermal component. This was required *in addition* to the BB modelling the γ-ray data for a broad-band good fit. Note, however, that a cut-off power law plus a single BB ($kT = 0.83^{+0.06}_{-0.05}$ keV) is a much better fit to the γ-ray plus X-ray data, with χ^2/d.o.f. = 715/555, compared to 825/554 for the model comprising a 'normal' power law plus two BB components.

2.1.1 *Spectral lag analysis*

Long GRBs are known to show spectral lags, i.e. there is a difference in arrival time between the high-energy and lower energy photons. In the case of short GRBs, negligible spectral lag is found (e.g. Norris & Bonnell 2006), at least above ∼15–25 keV. Following Ukwatta et al. (2010), spectral lags were estimated for GRB 090618. At around 40 s after the trigger time, the initial, smooth, lower count-rate pulse ends and the second emission interval, consisting of the bright, overlapping peaks, begins; thus, the data from −10–40 and 40–200 s were considered separately. The energy channels used were 15–25, 25–50, 50–100 and 100–350 keV, and a positive lag corresponds to the higher energy photons arriving earlier. It was found that both episodes showed significant positive spectral lags, but that the earlier interval shows a lag about a factor of 6 longer than for the second interval (a lag of ∼1.5–6 s, depending on the channels compared, rather than 0.2–1 s for the later emission).

One possibility for the cause of lags is spectral evolution: as $E_{\rm peak}$ moves through the bandpass, the ratio of the emission at different energies will vary. Fig. 2 shows how $E_{\rm peak}$ changes for GRB 090618. There is a rapid fall in the peak energy during the initial emission episode, which could be causing the large (few second) lag seen at this time. During the second interval, $E_{\rm peak}$ first moves back to higher values before decreasing again, because of the flaring activity; this could therefore diminish the mean lag over this time.

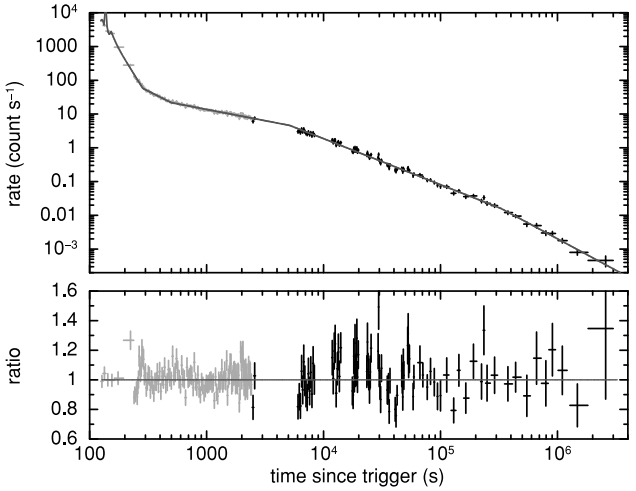

Figure 3. 0.3–10 keV *Swift*-XRT light curve: WT data in grey (200 count bin^{-1}, using dynamic binning; see Evans et al. 2009) and PC in black (100 count bin^{-1}). The decay has been fitted with a series of power-law and flare components (see Table 1 for details). The lower panel shows the ratio between the data and the model.

There is a lag–luminosity relationship, whereby bursts with higher luminosities tend to show shorter lags (Norris, Marani & Bonnell 2000; Ukwatta et al. 2010). The separate lag–luminosity results found for each interval of emission for GRB 090618 are consistent with the sample of other *Swift* bursts shown in figs 6–11 of Ukwatta et al. (2010). Hakkila et al. (2008) found that the lag–luminosity relation applied to individual pulses within *BATSE*[25] bursts and that long-lag pulses often precede short-lag ones. They also found that the count-rate amplitude is lower for pulses with longer lags and that pulse width increases with increasing lag. GRB 090618 is consistent with all of these results, although the second episode considered for GRB 090618 actually comprises a number of pulses itself.

2.2 X-rays

Following the slew of the spacecraft, *Swift*-XRT started collecting data 125 s after the burst trigger, initially centroiding on a 0.1 s Short Image Mode frame (Schady et al. 2009b). Fig. 3 shows the entire XRT data set, spanning 125 s to 2.9 Ms after the trigger. In total, 2.3 ks of WT mode data were collected, followed by almost 338 ks of PC mode data. The light curve can be modelled by a power-law decay with five different slopes (simply parametrizing the smooth variation in decay slope with a series of sharply broken power laws; Table 1), beginning with a very rapid decline of $\alpha = 5.59^{+0.10}_{-0.09}$. Each of these changes in slope is significant at >99.99 per cent confidence. There are small flares superimposed on the underlying decay until about 180 s after the trigger, which can be modelled with a 'burst' component (a linear rise, followed by an exponential decay). The three strongest flares peak at 130^{+2}_{-5}, 136^{+4}_{-11} and 151^{+5}_{-1} s after the trigger, although only the flare at ∼151 s is actually statistically significant at >99 per cent; the relevant section

[25] *Burst And Transient Source Experiment*

Table 1. Temporal (X-ray and UV/optical) and spectral (X-ray) fits; the X-ray and UV data were fitted separately. All the spectral fits include Galactic $N_{\rm H} = 5.8 \times 10^{20}$ cm^{-2} and an intrinsic column of $zN_{\rm H} = (1.82 \pm 0.08) \times 10^{21}$ cm^{-2}. See text for UVOT fits including a host galaxy contribution.

Temporal parameter	X-ray value	UV/optical value	$\Gamma_{\rm X}$
α_1	$5.59^{+0.10}_{-0.09}$	–	$1.50^{+0.16}_{-0.15}$*
$T_{\rm break,1}$ (s)	278^{+7}_{-5}	–	
α_2	$1.87^{+0.20}_{-0.19}$	–	2.00 ± 0.07*
$T_{\rm break,2}$ (s)	484^{+27}_{-28}	–	
α_3	0.67 ± 0.02	0.720 ± 0.002	2.07 ± 0.02
$T_{\rm break,3}$ (s)	5150^{+237}_{-367}	7485 ± 21	
α_4	1.36 ± 0.02	1.055 ± 0.001	1.96 ± 0.03
$T_{\rm break,4}$ (s)	$(3.05^{+0.73}_{-0.96}) \times 10^5$	$(4.85 \pm 0.02) \times 10^4$	
α_5	$1.88^{+0.16}_{-0.15}$	1.62 ± 0.02	1.91 ± 0.16

*Fit includes a BB component.

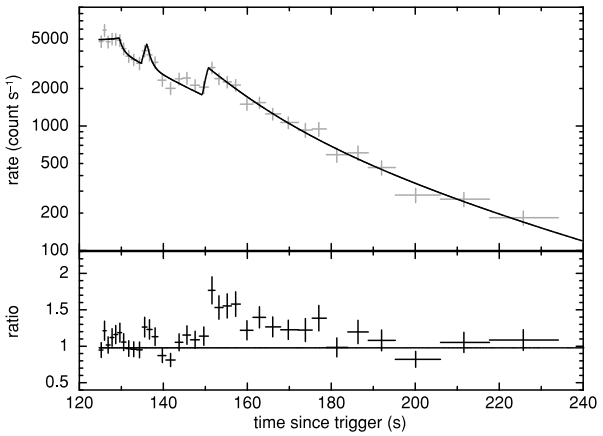

Figure 4. Early flares in the WT data. The light curve was modelled with an underlying power law plus three flare components; the normalizations of the flares were then set to zero to produce the bottom panel of this plot.

of the light curve is shown in Fig. 4. This final best-fitting model (including four breaks and three flares; Fig. 3) provides a reduced χ^2 value of 1.02 ($\chi^2 = 1309$ for 1289 d.o.f.).

Peaking above 6000 count s^{-1}, GRB 090618 was the brightest burst detected by the XRT by that date. However, settling mode XRT data are now routinely obtained, allowing the collection of X-ray data even more rapidly after the GRB; in this way, GRB 100621A has surpassed GRB 090618 as the burst with the highest detected XRT count rate. GRB 090618 does, however, have a remarkably high X-ray count rate and corresponding fluence throughout its 'plateau' phase (see, e.g. Evans et al. 2009) and remained in WT mode until 2.5 ks after the trigger. Fig. 5 plots GRB 090618 together with the 12 other bursts which have a peak XRT count rate of above 1000 count s^{-1}. It can be seen that GRB 090618 (black filled circles) peaks above all the other bursts, even GRB 080319B, the so-called 'naked-eye' burst (Racusin et al. 2008); only the settling mode points (the first five points in the light curve, plotted with cyan star symbols) obtained for GRB 100621A reach a higher count rate. GRB 080319B was, however, at a higher redshift ($z = 0.937$; Cucchiara & Fox 2008; Vreeswijk et al. 2008a,b), so was more X-ray luminous. We note that these count rates are based on the standard binning within the light-curve repository (Evans et al. 2007, 2009); if shorter time bins were considered, some of the objects might reach even higher rates.[26]

Fig. 6 shows the 10-keV flux density light curve for the first snapshot, obtained from the Burst Analyser website (Evans et al. 2010), together with the BAT and XRT hardness ratios over 50–150 keV/15–50 keV and 1.5–10 keV/0.3–1.5 keV, respectively. The hardness ratio panels show clear spectral evolution throughout the BAT-detected emission (see also Fig. 2) and until the end of the steep decay seen in the XRT.

2.2.1 Thermal emission

GRBs 060218 and 100316D are both examples of GRBs with associated SNe for which thermal components were required to model the early X-ray spectra [Campana et al. 2006; Starling et al. 2011 – although Fan et al. (2011) dispute the existence of the BB, despite their fits showing a marked improvement in the χ^2 statistic following the addition of the component] in addition to the standard non-thermal synchrotron (power-law) emission. In light of this, a search was made for similar thermal emission in GRB 090618.

Results of fitting time-sliced XRT spectra with both absorbed power laws and absorbed power law plus BB models are given in Table 2. The Galactic absorbing column was fixed at 5.8×10^{20} cm^{-2} (Kalberla et al. 2005). In addition, an intrinsic (at $z = 0.54$) column of $(1.82 \pm 0.08) \times 10^{21}$ cm^{-2} was estimated from the late-time *XMM–Newton* spectra (discussed below) and fixed at this value in all fits. We note that the additional BB component was present when the spectra were modelled using the currently released version of the *Swift* software (build 3.7), as well as when using the new, pre-release gain file.

The BB component appears to be significant [>99.99 per cent confidence from the F-test, although Protassov et al. (2002) highlight that the F-test should not strictly be used in such circumstances, and we present below a more detailed method of testing] during the steep decay phase of the light curve. There is also evidence for this component in the later (275–2453 s) WT data, although the fractional flux is very much lower (∼4 per cent compared to ∼20 per cent; see below). Fig. 7 shows the unfolded WT spectra from the steep decay, clearly demonstrating the cooling of the thermal emission over time. Fig. 8 plots the spectral parameters from the power law plus BB fits given in Table 2. Using a flat Universe cosmology with $\Omega_{\rm M} = 0.27$, $\Omega_{\rm vac} = 1 - \Omega_{\rm M} = 0.73$ and a Hubble constant of $H_0 = 71$ km s^{-1} Mpc^{-1}, the redshift of 0.54 corresponds to a luminosity distance of $D_{\rm L} = 3098.7$ Mpc. This allows us to convert the normalization of the BB component fitted to each spectrum to a luminosity and emitting radius, both of which are included in Fig. 8.

As shown in Fig. 4, there is low-level flaring activity at the start of the X-ray light curve. Spectra including (125–180 s after the trigger) and excluding (180–275 s) the flaring period were also extracted in order to ensure that any thermal emission found was not simply a symptom of a changing power law caused by the flares; both of these spectra were significantly better fitted with an additional thermal component, lending weight to the detection.

In order to test the significance of this thermal component more rigorously, 10 000 spectra based on the single power-law fit to the time-averaged, non-flaring WT data (180–275 s after the trigger) were simulated. These simulated spectra were then each fitted with

[26] For example, GRB 100621A actually peaked at 1.43×10^5 photon s^{-1}; see http://www2.le.ac.uk/ebulletin/news/press-releases/2010-2019/2010/07/nparticle.2010-07-15.0451482526.

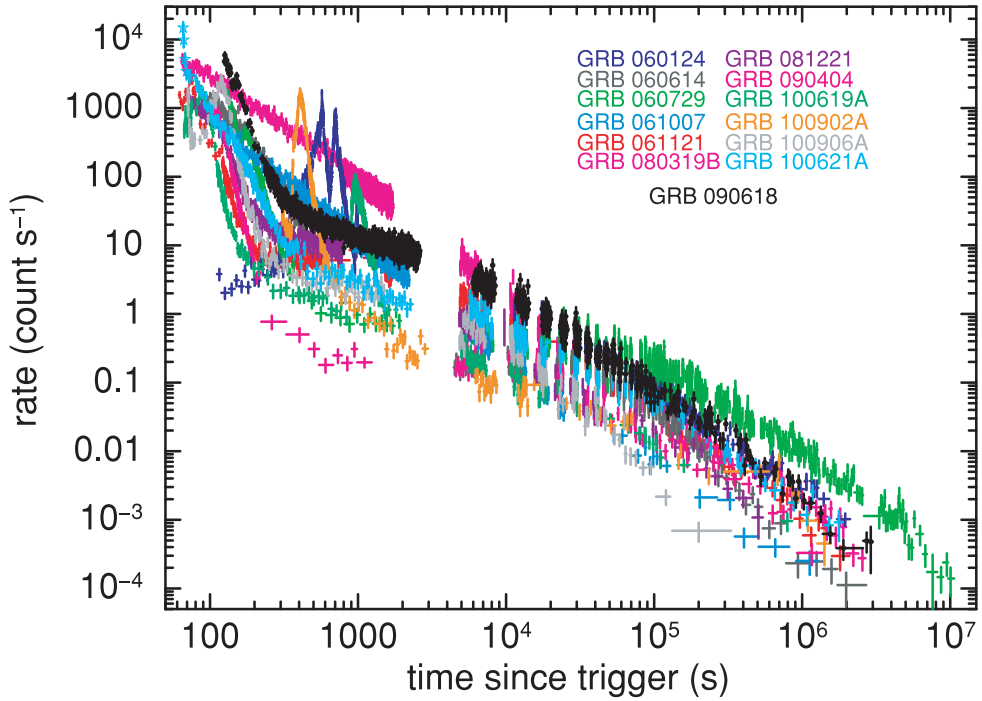

Figure 5. The *Swift*-XRT light curves which peak above 1000 count s^{-1}. The cyan star symbols signify the data were collected in settling mode. With the exception of these first few data points collected for GRB 100621A, GRB 090618 (plotted as black filled circles) reaches the highest X-ray count rate.

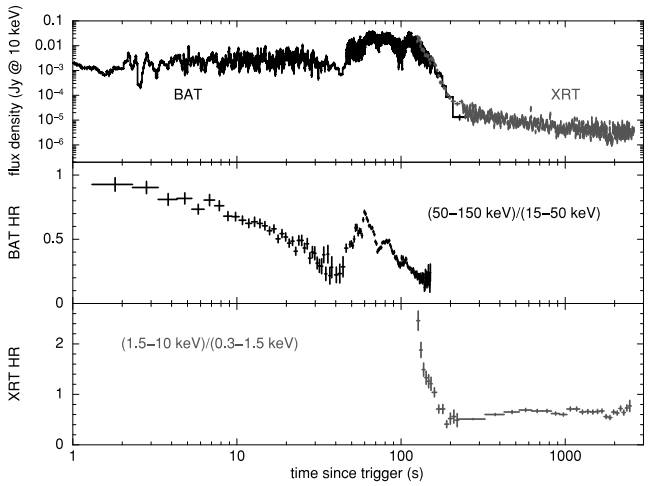

Figure 6. BAT and XRT 10 keV flux density light curve and hardness ratios for the early time data collected for GRB 090618.

an absorbed power law plus BB model to recover the chance probability that adding a thermal component actually improves the fit; see Hurkett et al. (2008) for details on the methodology. Not one of the simulated spectra showed a significant improvement in the fit statistic when the BB was included, implying that the component found in the time-averaged spectrum is significant at the $>4\sigma$ level. This test therefore provides a high degree of confidence in the presence of a thermal component in the X-ray spectra at early times.

An observation of GRB 090618 was performed by *XMM–Newton* (Jansen et al. 2001) about 19 ks after the GRB trigger (Campana 2009) and is used by Campana et al. (2011) to probe the ambient medium of the burst. We note that they find a slightly higher value of the column density (even with the assumption of solar metallicity), but that this measurement does not adversely affect our detection of a thermal component in the early-time spectra. The flux determined from the EPIC[27] pn (Strüder et al. 2001) and MOS (Turner et al. 2001) data is in complete agreement with the measurements by the XRT. The fits to the EPIC data have been included in Table 2; there is no evidence for significant thermal emission in these spectra, ∼20–40 ks after the trigger. Similarly, the *Swift*-PC data from the second snapshot onwards are well fitted by single absorbed power laws. Although a small amount of PC data was collected at the end of the first snapshot, there were insufficient counts (once the piled-up core had been excluded) to constrain any model more complicated than a single power law.

The bottom panel of Fig. 8 shows that the percentage of the 0.3–10 keV flux contributed by the BB (comparing unabsorbed fluxes) declines slightly from ∼21 to 18 per cent. Starling et al. (in preparation) found the BB to contribute a higher percentage (∼51 per cent) of the flux in GRB 100316D, while Campana et al. (2006) found that the BB contribution in GRB 060218 increased from about 20 per cent at the start of the observations to being the dominant component at the end of the steep decay seen in the XRT data.

In Section 2.1, the BAT spectra were fitted with a quasi-thermal model, to test for possible photospheric emission (Ryde 2004; Ryde & Pe'er 2009). These BB components have much higher temperatures (10 s of keV) than the thermal emission discussed in this section (and are typically poorer fits to the γ-ray spectra than a cut-off power law, anyway), although were found to be cooling over time, reaching ∼5 keV in the 130–160 s bin. However, when fitting the simultaneous γ-ray and X-ray data from 130–160 s after the trigger, both a BB component to account for the curvature in the γ-ray spectrum *and* a cooler BB for the XRT data were required, as mentioned in Section 2.1, with a decrease in χ^2 of 398

[27] European Photon Imaging Camera

Table 2. Time-sliced X-ray spectra. All the spectral fits include Galactic $N_{\rm H} = 5.8 \times 10^{20}$ cm^{-2} and an intrinsic column of $zN_{\rm H} = (1.82 \pm 0.08) \times 10^{21}$ cm^{-2}. There is no evidence for significant thermal emission in the late-time *Swift*-PC or *XMM* spectra.

Time since trigger (s)	Mode/instrument	Model	$\Gamma_{\rm X}$	BB kT (keV)	BB norm.[a]	χ^2/d.o.f.	F-test sig.
125–165	Swift-WT	PL	1.29 ± 0.06			191.3/149	
125–165	Swift-WT	PL+BB	$1.23^{+0.20}_{-0.19}$	$0.97^{+0.28}_{-0.20}$	$0.80^{+0.36}_{-0.27}$	163.6/147	>0.9999
165–205	Swift-WT	PL	1.921 ± 0.043			168.5/137	
165–205	Swift-WT	PL+BB	$1.77^{+0.10}_{-0.12}$	$0.541^{+0.073}_{-0.056}$	$0.162^{+0.037}_{-0.035}2$	106.1/135	>0.9999
205–245	Swift-WT	PL	2.08 ± 0.05			134.4/103	
205–245	Swift-WT	PL+BB	$1.84^{+0.12}_{-0.13}$	$0.341^{+0.039}_{-0.033}$	0.053 ± 0.018	111.8/101	>0.9999
245–275	Swift-WT	PL	2.17 ± 0.05			141.8/106	
245–275	Swift-WT	PL+BB	$1.85^{+0.13}_{-0.14}$	0.285 ± 0.026	0.027 ± 0.008	116.9/104	>0.9999
275–2453	Swift-WT	PL	1.982 ± 0.015			469.9/434	
275–2453	Swift-WT	PL+BB	1.939 ± 0.028	$0.45^{+0.09}_{-0.05}$	$(8.5^{+3.0}_{-2.8}) \times 10^{-4}$	442.6/432	>0.9999
5.96×10^3–3.01×10^5	Swift-PC	PL	1.922 ± 0.039			242.5/201	
3.07×10^5–2.99×10^6	Swift-PC	PL	$1.82^{+0.19}_{-0.18}$			26.3/27	
2.05×10^4–4.25×10^4	XMM-PN	PL	2.000 ± 0.014			697.5/696	
1.92×10^4–4.22×10^4	XMM-MOS1	PL	1.938 ± 0.018			299.9/332	
1.92×10^4–4.22×10^4	XMM-MOS2	PL	1.922 ± 0.018			365.5/312	

[a]BB normalization $= L_{39}/D_{10}^2$, where L_{39} is the source luminosity in units of 10^{39} erg s^{-1} and D_{10} is the distance to the source in units of 10 kpc.

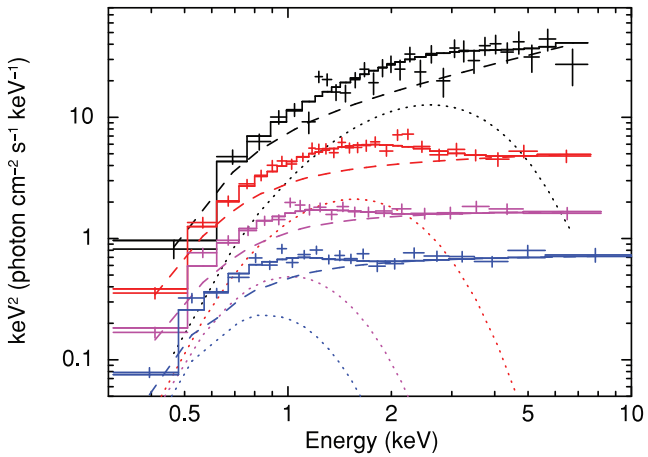

Figure 7. Time-sliced WT data from the steep decay phase fitted with the model comprising power-law (dashed lines) and BB (dotted lines) components. The spectra correspond to 125–165 (black), 165–205 (red), 205–245 (magenta), 245–275 s (blue) after the trigger, during which time the BB can clearly be seen to be cooling. The ordinate axis $[E^2F(E)]$ is equivalent to νF_ν.

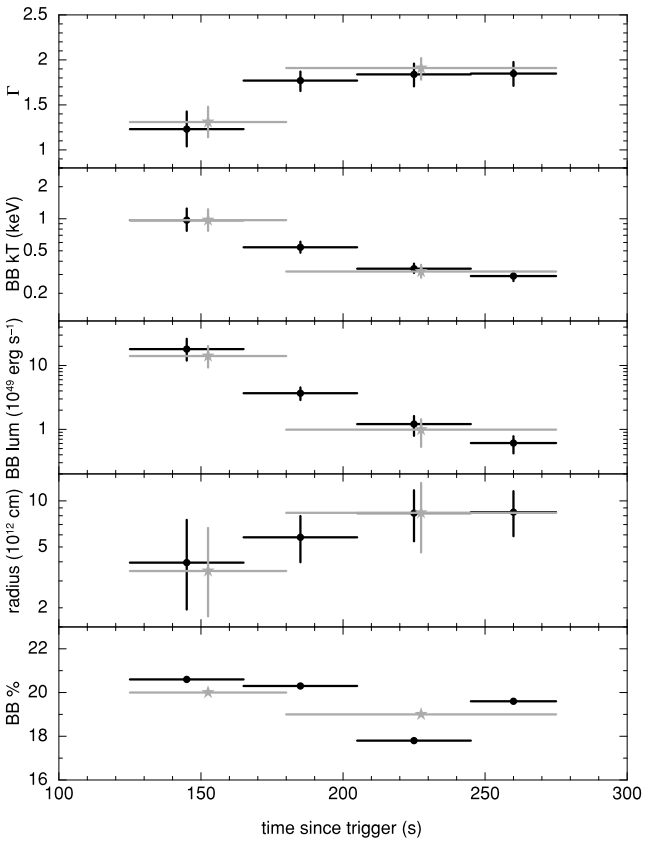

Figure 8. BB parameters from the XRT spectral fits shown in Fig. 7 (black circles). The BB cools and expands over time, contributing ∼21–18 per cent of the 0.3–10 keV flux. The grey (starred) points show spectra from the time during which there are flares in the X-ray light curve (125–180 s) and after the flaring activity has stopped (180–275 s).

for 2 d.o.f. This implies that the thermal component in the XRT data is not likely to be of the same photospheric origin. We do reiterate, however, that a cut-off power-law fit to the γ-ray data is a significant improvement over a power law plus thermal component combination, meaning that a cut-off power law plus BB better fits the complete BAT+XRT energy range. The temperature of this single BB component is ∼1 keV; that is, the component is fitting the X-ray data, rather than the γ-ray.

2.3 Optical and UV

Swift-UVOT detected the afterglow of GRB 090618 in all filters (Schady 2009). The light curves have been normalized to the white filter and are plotted, together with the *ROTSE* data, in Fig. 9. UVOT photometry was performed on the photometric system described in Poole et al. (2008). There is an uncertainty of ∼0.03 mag on the zero-point which has not been included in the plotted error bars. Note that the unfiltered *ROTSE* light curve has not been normalized to align with the UVOT, since it already seems in quite good agreement with the broad-band white filter. The first *ROTSE* point at 37.5 s after the trigger is a 3σ upper limit at 15.6 mag, demonstrating that

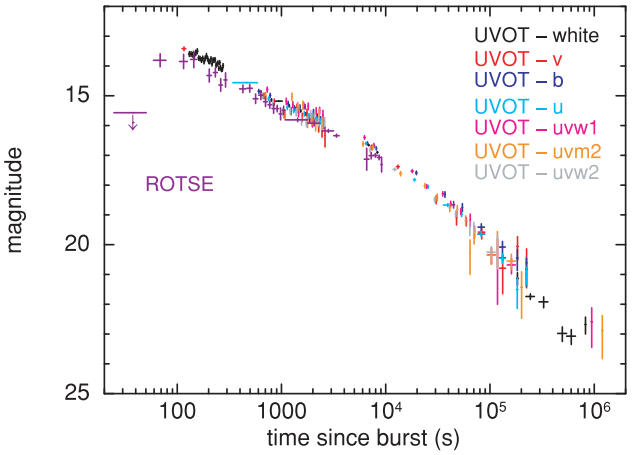

Figure 9. UVOT (normalized to white) optical and UV and *ROTSE* light curves of the afterglow of GRB 090618.

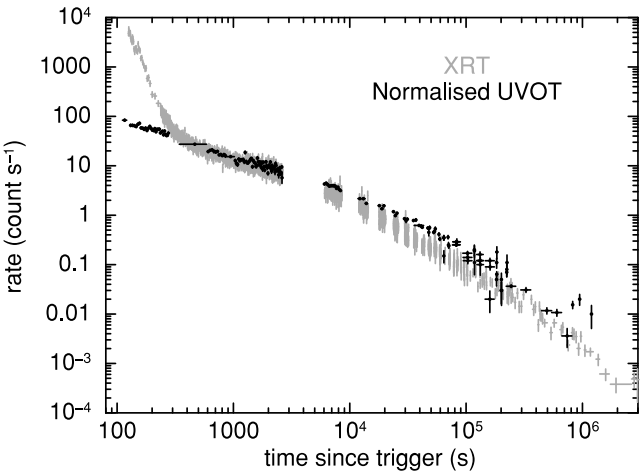

Figure 10. XRT and normalized UVOT count rates. The *v*, *b*, *u*, *uvw*1, *uvm*2 and *uvw*2 light curves were all normalized to the white filter, which was then scaled down by a factor of 7.2 to align with the XRT plateau at 2.6 ks.

the optical afterglow was initially faint, before it rose to a peak sometime after 69 s.

A UV bump, likely associated with SN shock breakout, was clearly seen in the optical light curve of GRB 060218 around 30 ks after the burst (Campana et al. 2006), though see Section 3.2 for a discussion on the viability of this explanation of the additional component. The UVOT data collected for the higher redshift GRB 090618 ($z = 0.54$ compared to 0.033 for GRB 060218; Mirabel & Halpern 2006), however, are dominated by the bright GRB optical afterglow. Cano et al. (2011) present additional optical data for GRB 090618 which show an SN rise starting about 10 days (8.6×10^5 s) after the trigger, around the time UVOT observations ceased, although the final points in Fig. 9 are higher than expected from an extrapolation of the power-law decay. Thus, when fitting the UVOT light curve to characterize the afterglow, data after 8×10^5 s were excluded to avoid any possible SN contamination. In the following work, the filter-normalized count-rate light curve was used. A singly broken power-law model is a poor fit to the data, and a significant improvement is found when either a smooth break (as used in Cano et al. 2011) replaces the sharp one (with an F-test probability of 10^{-6}) or a second sharp break is inserted (F-test probability 10^{-7}). The fit for the doubly broken power law is given in Table 1 for direct comparison with the XRT data. The smoothly broken power-law fit results in a smoothness parameter, s, of $\sim$1.5, $\alpha_1 = 0.72 \pm 0.01$, $T_{\rm break} = (3.0 \pm 0.1) \times 10^4$ s and $\alpha_2 = 1.68 \pm 0.02$. In both cases (two sharp breaks or a single smooth one), the data before 300 s are slightly underpredicted, which could mean that they contain some contamination from a further component, most likely the prompt emission. A direct comparison between the XRT and UVOT fits is presented in Section 2.4.

To quantify the effect of an underlying host galaxy contribution in the late-time light curve, we added a constant value fixed at the level of the faintest UVOT white filter observation. This resulted in an increase in the final decay slope to $\alpha_2 = 1.77 \pm 0.03$ in the smoothly broken power-law model, with change in the smoothness to $s \sim 1.3$ and $T_{\rm break} = (3.3^{+0.2}_{-0.1}) \times 10^4$ s; the final slope in the doubly broken power-law model became 1.66 ± 0.01. These results are in broad agreement with the ground-based optical afterglow decay reported in Cano et al. (2011; their fig. 5).

We note that, while this final break time is not in agreement with the X-ray value (Table 1), the UVOT data are sparse and show significant scatter at this time. This is discussed further in Section 2.4.

2.3.1 *Onset of the afterglow*

The early non-detection by *ROTSE* allows us to place constraints on the time of the peak of the optical afterglow and, thus, the initial Lorentz factor, Γ_0 (Molinari et al. 2007). Taking the peak time to be 92 s (midway between the two earliest *ROTSE* detections) and $E_{\rm iso} = 2.5 \times 10^{53}$ erg (see Section 2.1), we find $\Gamma_0 = 435$ (assuming typical values for the radiative efficiency, η, and the particle density, n, of 0.2 and 1 cm^{-3}, respectively; Bloom, Frail & Kulkarni 2003), similar to values found for other bursts (Molinari et al. 2007; Page et al. 2009a; Xue, Fan & Wei 2009).

2.4 Multiwavelength comparison

The initial decay seen by the UVOT is similar to that of the contemporaneous XRT plateau phase (α_3 in Table 1); however, beyond about 5 ks after the trigger, the X-ray data fade more rapidly than do the optical and UV. This is demonstrated by Fig. 10, where the UVOT count rate light curves have been normalized to align with the XRT rate at the end of the plateau phase ($\sim$2.6 ks after the trigger).

In Section 2.3, it was found that a single, smoothly broken power law was as good a fit to the UVOT data as two sharp breaks over the same time interval. For comparison, the XRT curve was also fitted with a smooth break at later times; data after $\sim$500 s were considered, to avoid the early steep decay. Again, a smooth break was found to be an acceptable fit, with $\alpha_1 = 0.59^{+0.06}_{-0.10}$ before a break time of $7.0^{+1.0}_{-1.2}$ ks, followed by $\alpha_2 = 1.55^{+0.05}_{-0.04}$, for a smoothness parameter of $\sim$1.4. However, the time of this smooth break is far earlier than that found for the UVOT data (3×10^4 s) and the fit is much worse if the break time is fixed at the UVOT value (F-test improvement of 10^{-16} for the XRT free fit over the UVOT value); similarly, the UVOT result is poorer if fixed at the XRT break time.

Cano et al. (2011) claim an achromatic break at $\sim 4.3 \times 10^4$ s. Although the fits presented here are not obviously in agreement with this, the possibility of such a break was investigated. Keeping the final (sharp) break time tied between the XRT and UVOT light curves, but allowing all other parameters to vary independently, provides an acceptable fit (χ^2 is only 9 higher for 1 d.o.f.; allowing this break time to vary is thus only significant at the 98.6 per cent level – less than 3σ), with $\alpha_{\rm XRT} = 1.55 \pm 0.03$ and $\alpha_{\rm UVOT} = 1.62^{+0.05}_{-0.04}$

after $(5.2 \pm 0.4) \times 10^4$ s. These decay slopes are just consistent at 90 per cent, suggesting that the change in slope of the light curve *could* be caused by a jet break, although a decay of $\alpha \sim 1.6$ is less steep than typically expected ($\sim t^{-2}$ is expected post-jet-break; Zhang & Mészáros 2004). Residual curvature can be seen in the X-ray light curve if the break time is tied with that in the UVOT, which is removed if the free fit given in Table 1 is used.

Assuming the break at $(5.2 \pm 0.4) \times 10^4$ s is, indeed, caused by a jet, the opening angle can be calculated to be 4.°2, corresponding to a beaming-corrected energy (taking $E_{\rm iso}$ to be 2.5×10^{53} erg from Section 2.1) of $E_\gamma = 6.8 \times 10^{50}$ erg (Sari, Piran & Halpern 1999; Frail et al. 2001).

Taking $E_{\rm peak} = 211$ keV (from the cut-off power-law fit to the T_{90} spectrum, these data are consistent with the Ghirlanda correlation (Ghirlanda, Ghisellini & Lazzati 2004) relating E_γ and $E_{\rm peak}$.

An upper limit to the energy can be determined by considering the final (later) break time obtained from fits to the XRT alone (as given in Table 1). This suggests that the opening angle could be as large as 8.°2, giving an estimated E_γ of up to 2.6×10^{51} erg. Considering just the XRT fit, $\alpha_{\rm XRT,5} = 1.88^{+0.16}_{-0.15}$ and $\beta_{\rm X} = 0.91 \pm 0.16$, meaning that $\alpha = 2\beta$ (within the uncertainties), in agreement with the closure relation for post-jet-break decay where $\nu > \nu_{\rm c}$ (Zhang & Mészáros 2004). The slope determined from the fit to the XRT and UVOT data with a common break time ($\alpha_{\rm XRT} \sim 1.55$) is too shallow to satisfy the jet–break closure relation.

There are different explanations for the lack of obvious achromatic breaks in most light curves from the *Swift* era, from the breaks being 'hidden' within the data (Curran, van der Horst & Wijers 2008) to structured (e.g. Rossi, Lazzati & Rees 2002; Granot 2005) or multiple (e.g. Racusin et al. 2008) jet systems. Van Eerten et al. (2011) show that jet breaks can be chromatic across the self-absorption break, with the possibility of the radio jet break being postponed by up to several days; however, their simulations do not find a large difference between the X-ray and optical jet break times.

3 DISCUSSION

3.1 Comparison with GRBs 060218 and 100316D

Despite also being a GRB–SN with early thermal emission, GRB 090618 is somewhat different from GRB–SNe 060218 and 100316D, from a *Swift* point of view. GRBs 060218 and 100316D both showed soft γ-ray spectra, with low $E_{\rm peak}$ values and few counts above 100 keV, whereas GRB 090618 is typical of BAT-detected bursts (see Sakamoto et al. 2008). GRB 090618 also showed a much shorter duration of $T_{90} \sim 113$ s, compared to 2100 and >1300 s for GRBs 060218 and 100316D, respectively. We note in passing that the current record holder for the duration is GRB 090417B with a T_{90} of at least ∼2130 s (Holland et al. 2010), while GRB 101225A also had an extreme duration, with $T_{90} > 1650$ s (this was a very long 1088-s image trigger in the BAT; Cummings & Sakamoto 2010; Racusin et al. 2011). GRB 090417B does not show signs of an accompanying SN in the optical, however, despite being at low redshift ($z \sim 0.345$ for the galaxy within the XRT error circle; Berger & Fox 2009). A faint photometric SN was identified for GRB 101225A (Thöne et al. 2011b), and there is evidence for a thermal signature in the X-ray data for this object, as first mentioned by Campana (2010). We do point out, however, that there is uncertainty about the nature of so-called GRB 101225A (e.g. Thöne et al. 2011a, though see also Thöne et al. 2011b).

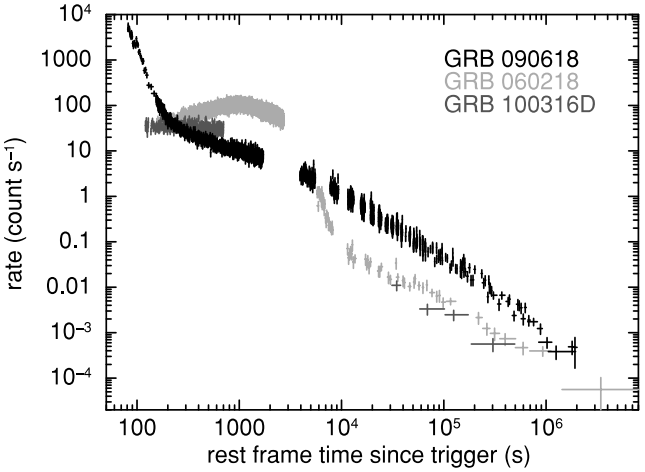

Figure 11. Comparison of the GRB 090618 *Swift*-XRT light curve with those of the other two GRB–SNe where there was an obvious thermal signature in the early X-ray spectra. GRBs 060218 and 100316D have unusual light curves, while GRB 090618 is much more 'canonical'. The light curves are plotted as time since trigger in the rest frame in each case ($z = 0.54$, 0.0331 and 0.0591 for GRBs 090618, 060218 and 100316D, respectively).

The GRB 090618 X-ray light curve shows an early steep decay (Schady, Baumgartner & Beardmore 2009a), while GRBs 060218 and 100316D initially showed rising/constant X-ray emission, respectively (Campana et al. 2006; Starling et al. 2011; see also Fig. 11). This makes GRB 090618 more representative of the 'canonical' light curve discussed by Nousek et al. (2006) and Zhang et al. (2006), although see Evans et al. (2009) for different light curve morphologies. As fig. 7 in Starling et al. (2011) demonstrates, GRBs 060218 and 100316D are actually in the minority for GRB–SN X-ray light-curve profiles.

GRB 090618 showed a bright, fading optical afterglow before any SN component was identified, while no such afterglow was found for the other two bursts. GRB 090618, while a relatively low redshift object at $z = 0.54$, is still noticeably more distant than GRB 060218 ($z = 0.0331$) and GRB 100316D ($z = 0.0591$). GRBs 060218 and 100316D are both underluminous (typically the case for spectroscopically confirmed GRB–SNe), while this is not the case for GRB 090618, with $E_{\rm iso} \sim$ a few $\times 10^{53}$ erg; the SN associated with GRB 090618 was found through photometry, not a spectroscopic analysis, however. GRB 101219B is another luminous ($E_{\rm iso} \sim 10^{51}$ erg) GRB with a detection of a spectroscopic SN (Sparre et al. 2011), and evidence for thermal emission in the X-ray band will be presented by Starling et al. (in preparation). This burst lies at a redshift of $z = 0.55$, similar to GRB 090618.

Both Campana et al. (2006) and Starling et al. (2011) found that the temperature of the BB components remained close to constant (for the first few thousand seconds in GRB 060218 and for the time of detection for GRB 100316D), between ∼0.1 and 0.2 keV. There is evidence for cooling of the thermal emission in the case presented here, however, from ∼1 keV at the start of the observation to ∼0.3 keV after a few hundred seconds. The emitting radius does not appear to expand much during this time, while Campana et al. (2006) found an increasing radius for GRB 060218 starting at $\sim 5 \times 10^{11}$ cm, smaller than measured here; their final radius measurement comes from the fitting of the UVOT data at $>10^5$ s after the trigger and is significantly larger, at a few $\times 10^{14}$ cm.

It has been considered (Toma et al. 2007) that long-duration, low-luminosity bursts could be signatures of neutron star, rather than black hole, central engines, with just mildly relativistic jets. GRB 090618 is unlikely to come under this heading, though, given that its isotropic luminosity is about 4 orders of magnitude higher than GRBs 060218 and 100316D.

Li (2006) claims a correlation between the rest-frame $E_{\rm peak}$ of a GRB and the peak bolometric magnitude of its corresponding SN. However, only four systems were considered (GRBs 980425, 030329, 031203 and 060218), making the correlation rather tenuous. GRB 090618 does not lie on the purported trend, showing a much lower $E_{\rm peak}$ than would be expected from the peak bolometric magnitude of -19.75 (taken from Cano et al. 2011) if the correlation were confirmed.

3.2 What causes the thermal emission?

Campana et al. (2006) and Waxman, Mészáros & Campana (2007) suggest that the thermal emission seen in the spectra of GRB 060218 is due to the SN shock breakout from a dense stellar wind, implying that the progenitor was a Wolf–Rayet type star. However, work by Ghisellini, Ghirlanda & Tavecchio (2007a,b), Li (2007) and Chevalier & Fransson (2008) has cast doubt on this explanation, saying that the energetics are not feasible, with the energy of the BB component being too large. In the case presented here, the estimated BB luminosities are even larger, up to 10^{50} erg s^{-1}. Fan, Piran & Xu (2006) believe that there is unlikely to be a dense wind surrounding the progenitor and so consider that the thermal emission may arise from the shock-heated stellar envelope.

Waxman et al. (2007) state that, for a SN shock breakout, the photospheric radius increases with time as $R \propto t^{0.8}$ and that the corresponding temperature falls as $T \propto t^{-0.5}$ (see also Chevalier & Fransson 2008). While the measurements of the expanding radius we present in Fig. 8 do approximately follow $t^{0.8}$ (although, within the errors, they are also consistent with a constant value of $\sim$6.5 $\times$ 10^{12} cm), the temperatures found decrease more rapidly than the proposal of Waxman et al. If the radius really is almost constant, this would imply that the emission seen was not caused by an explosive shock breakout, however. An aspherical explosion can explain the relatively long durations of the thermal X-ray emission (Waxman et al. 2007) and, in GRB 090618, the BB is only strongly detected for the first $\sim$300 s, a much shorter interval than in GRB 060218.

On a related note, Soderberg et al. (2008) present observations of SN 2008D (which did not have an accompanying GRB) showing an X-ray outburst at the time of the SN explosion which they attribute to shock breakout (see also Chevalier & Fransson 2008), predicting that such outbursts should occur for every core-collapse SN. In this case, the spectrum of the X-ray outburst detected was well fitted by a simple power-law model, rather than a thermal component, which Soderberg et al. (2008) explain as bulk Comptonization of the photons across the shock front, with the thermal component lying below the XRT band. Couch et al. (2011) discuss how an aspherical shock breakout could also explain the X-ray emission seen in this object, finding that the spectrum is not well fitted by a single temperature and radius BB, but is significantly more complex.

Although SNe associated with GRBs have sometimes been referred to as hypernovae because of their higher energy output, the SN accompanying GRB 060218 (known as SN 2006aj) was closer to a 'typical' Type Ibc, implying that that hypernovae may just represent the energetic end of the SN population (Li 2006; Mazzali et al. 2006). Cano et al. (2011) find that the SN accompanying GRB 090618 is similar to (hypernova) SN 1998bw/GRB 980425 in terms of its temporal evolution and brightness.

While the results from GRB 090618 presented here do not resolve the disagreement about the origin of the thermal emission, they do add to the melting pot of data. A systematic search for X-ray thermal emission in other GRB–SNe is in progress (Starling et al. in preparation), and this larger sample may provide firmer conclusions. Recent developments in theoretical calculations of shock breakout also provide further means of testing this suggestion (Balberg & Loeb 2011; Katz, Sapir & Waxman 2011; Sapir, Katz & Waxman 2011).

4 SUMMARY

GRB 090618 was a long burst, extremely bright in γ-rays and X-rays, with an isotropic energy release of $\sim$2.5 $\times$ 10^{53} erg. The γ-ray data are best fitted by a power law with a changing exponential cut-off signifying the peak energy of the spectrum moving through the band. There is a late-time break in the X-ray and optical temporal decay which is consistent with being achromatic, although the final decay is then shallower than usually expected for a post-jet-break decay and the fit improves if the break time is allowed to vary between the two data sets. Using this common break time, the beaming-corrected energy is estimated to be $\sim$6.8 $\times$ 10^{50} erg. If, however, the fit to the X-ray data alone is considered, the later break time suggests the beaming-corrected energy could be as high as 2.6 $\times$ 10^{51} erg.

The early X-ray spectra show good evidence for a thermal component in addition to the standard power-law continuum, which could be related to shock breakout of the (photometric) SN detected in the system, although this is by no means certain. GRB 090618 is, however, far more typical of 'normal' bursts than the previous GRB–SNe with thermal X-ray emission (i.e. GRBs 060218 and 100316D), in terms of both its γ-ray (T_{90}, $E_{\rm peak}$, energy release) and X-ray (overall shape of the light curve) parameters. It has often been suggested (e.g. Zeh, Klose & Hartmann 2004) that an SN component could be present in most long GRBs. Zhang (2011) points out that previously the only typical GRB with a robust SN association was GRB 030329, while the other objects are low-luminosity, nearby bursts and could, therefore, be part of a different population. More recently, Sparre et al. (2011) report the spectroscopic detection of SN 2010ma associated with GRB 101219B, another long burst (at $z = 0.55$) with a 'normal' isotropic energy ($\sim$4 $\times$ 10^{51} erg). The thermal X-ray component in GRB 090618 could provide a further link between the underluminous GRBs with spectroscopically associated SNe and the wider GRB population.

ACKNOWLEDGMENTS

The authors gratefully acknowledge support for this work at the University of Leicester by STFC and in Italy by funding from ASI. This work made use of data supplied by the UK *Swift* Science Data Centre at the University of Leicester. The *ROTSE* project is supported by the NASA grant NNX08AV63G and the NSF grant PHY-0801007. SMB acknowledges the support of a European Union Marie Curie European Reintegration Grant within the 7th Program under contract number PERG04-GA-2008-239176.

REFERENCES

Abdo A. A. et al., 2009, ApJ, 706, L138
Ackermann M. et al., 2011, ApJ, 729, 114
Amati L., 2006, MNRAS, 372, 233

Anupama G. C., Gurugubelli U. K., Sahu D. K., 2009, GCN Circ., 9576
Arnaud K. A., 1996, in Jacoby G., Barnes J., eds, ASP Conf. Ser. Vol. 101, Astronomical Data Analysis Software and Systems V. Astron. Soc. Pac., San Francisco, p. 17
Balberg S., Loeb A., 2011, MNRAS, 414, 1715
Band D. et al., 1993, ApJ, 413, 281
Barthelmy S. D. et al., 2005, Space Sci. Rev., 120, 143
Baumgartner W. H. et al., 2009, GCN Circ., 9530
Beardmore A. P., Schady P., 2009, GCN Circ., 9528
Berger E., Fox D. B., 2009, GCN Circ., 9156
Bissaldi E. et al., 2011, ApJ, 733, 97
Bloom J. S., Frail D. A., Kulkarni S. R., 2003, ApJ, 594, 674
Borgonovo L., Ryde F., 2001, ApJ, 548, 770
Burrows D. N. et al., 2005, Space Sci. Rev., 120, 165
Butler N. R., Kocevski D., 2007, ApJ, 663, 407
Caito L., Bernardini M. G., Bianco C. L., Dainotti M. G., Guida R., Ruffini R., 2009, A&A, 498, 501
Campana S., 2009, GCN Circ., 9516
Campana S., 2010, GCN Circ., 11501
Campana S. et al., 2006, Nat, 442, 1008
Campana S., D'Avanzo P., Lazzati D., Covino S., Tagliaferri G., Panagia N., 2011, MNRAS, in press
Cano Z., Guidorzi C., Bersier D., Melandri A., Steele I. A., Smith R. J., Mundell C., 2009, GCN Circ., 9531
Cano Z. et al., 2011, MNRAS, 413, 669
Carraminana A., Alvarez Ochoa C., Miramon G., 2009, GCN Circ., 9519
Cenko S. B., 2009, GCN Circ., 9513
Cenko S. B., Perley D. A., Junkkarinen V., Burbidge M., Miller K., 2009, GCN Circ., 9518
Chandra P., Frail D. A., 2009, GCN Circ., 9533
Chevalier R. A., Fransson C., 2008, ApJ, 683, L135
Couch S. M., Pooley D., Wheeler J. C., Milosavljević M., 2011, ApJ, 727, 104
Cucchiara A., Fox D. B., 2008, GCN Circ., 7456
Cucchiara A. et al., 2011, ApJ, in press (arXiv:1105.4915v2)
Cummings J. R., Sakamoto T., 2010, GCN Circ., 11504
Curran P. A., van der Horst A. J., Wijers R. A. M. J., 2008, MNRAS, 386, 859
Della Valle M. et al., 2006, Nat, 444, 1050
Evans P. A. et al., 2007, A&A, 469, 379
Evans P. A. et al., 2009, MNRAS, 397, 1177
Evans P. A. et al., 2010, A&A, 519, 102
Fan Y.-Z., Piran T., Xu D., 2006, J. Cosmol. Astropart. Phys., 09, 013
Fan Y.-Z., Zhang B.-B., Xu D., Liang E.-W., Zhang B., 2011, ApJ, 726, 32
Fatkhullin T., Moskvitin A., Castro-Tirado A. J., de Ugarte Postigo A., 2009, GCN Circ., 9542
Fernandez-Soto A., Peris V., Alonso-Lorite J., 2009, GCN Circ., 9536
Ford L. A. et al., 1995, ApJ, 439, 307
Frail D. A. et al., 2001, ApJ, 562, L55
Fynbo J. P. U. et al., 2006, Nat, 444, 1047
Galama T. J. et al., 1998, Nat, 395, 670
Galeev A. et al., 2009, GCN Circ., 9548
Gehrels N. et al., 2004, ApJ, 611, 1005
Gehrels N. et al., 2008, ApJ, 689, 1161
Ghirlanda G., Ghisellini G., Lazzati D., 2004, ApJ, 616, 331
Ghisellini G., Celotti A., Lazzati D., 2000, MNRAS, 313, L1
Ghisellini G., Ghirlanda G., Tavecchio F., 2007a, MNRAS, 375, L36
Ghisellini G., Ghirlanda G., Tavecchio F., 2007b, MNRAS, 382, L77
Goad M. R. et al., 2007, A&A, 468, 103
Golenetskii S. V., Mazets E. P., Aptekar R. L., Ilinskii V. N., 1983, Nat, 306, 451
Golenetskii S. et al., 2009, GCN Circ., 9553
Granot J., 2005, ApJ, 631, 1022
Guiriec S. et al., 2010, ApJ, 725, 225
Hakkila J., Giblin T. W., Norris J. P., Fragile P. C., Bonnell J. T., 2008, ApJ, 677, L81
Holland S. T. et al., 2010, ApJ, 717, 223
Hurkett C. P. et al., 2008, ApJ, 679, 587
Im M., Park W. K., Urata Y., 2009a, GCN Circ., 9522
Im M., Jeon Y.-B., Urata Y., 2009b, GCN Circ., 9541
Jansen F. et al., 2001, A&A, 365, L1
Kalberla P. M. W., Burton W. B., Hartmann D., Arnal E. M., Bajaja E., Morras R., Pöppel W. G. L., 2005, A&A, 440, 775
Kamble A., van der Horst A. J., Wijers R., 2009, GCN Circ., 9538
Katz B., Sapir N., Waxman E., 2011, preprint (arXiv:1103.5276v1)
Khamitov I. et al., 2009, GCN Circ., 9597
Klunko E., Volnova A., Pozanenko A., 2009, GCN Circ., 9613
Kono K., 2009, GCN Circ., 9570
Kono K. et al., 2009, GCN Circ., 9568
Kouveliotou C., Meegan C. A., Fishman G. J., Bhat N. P., Briggs M. S., Koshut T. M., Paciesas W. S., Pendleton G. N., 1993, ApJ, 413, L101
Li L.-X., 2006, MNRAS, 372, 1357
Li L.-X., 2007, MNRAS, 375, 240
Longo F. et al., 2009, GCN Circ., 9524
McBreen S., 2009, GCN Circ., 9535
Mallozzi R. S., Preece R. D., Briggs M. S., 2005, RMFIT: A Lightcurve and Spectral Analysis Tool. Univ. Alabama, Huntsville
Mangano V. et al., 2007, A&A, 470, 105
Mazzali P. A. et al., 2006, Nat, 442, 1018
Meegan C. A. et al., 2009, ApJ, 702, 791
Melandri A., Guidorzi C., Bersier D., Cano Z., Steele I. A., Mundell C. G., O'Brien P., Tanvir N., 2009, GCN Circ., 9520
Mirabel N., Halpern J. P., 2006, GCN Circ., 4792
Molinari E. et al., 2007, A&A, 469, L13
Morgan A. N., Klein C. R., Bloom J. S., 2009, GCN Circ., 9563
Nomoto K., Maeda K., Mazzakki P. A., Umeda H., Deng J., Iwamoto K., 2004, in Fryer C. L., ed., Astrophys. Space Sci. Library Vol. 302, Stellar Collapse. Kluwer, Dordrecht, p. 277
Nomoto K., Tominaga N., Tanaka M., Maeda K., 2007, in Antonelli L. A., Israel G. L., Piersanti L., Tornambè A., eds, AIP Conf. Proc. Vol. 924, The Multi-coloured Landscape of Compact Objects and their Explosive Origins. Am. Inst. Phys., New York, p. 108
Norris J. P., Bonnell J. T., 2006, ApJ, 643, 266
Norris J. P., Marani G. F., Bonnell J. T., 2000, ApJ, 534, 248
Nousek J. A. et al., 2006, ApJ, 642, 389
Ofek E. O. et al., 2007, ApJ, 662, 1129
Page K. L. et al., 2007, ApJ, 663, 1125
Page K. L. et al., 2009a, MNRAS, 395, 328
Page K. L. et al., 2009b, MNRAS, 400, 134
Perley D. A., 2009, GCN Circ., 9514
Poole T. S. et al., 2008, MNRAS, 383, 627
Pooley G., 2009a, GCN Circ., 9532
Pooley G., 2009b, GCN Circ., 9592
Preece R. D., Briggs M. S., Mallozzi R. S., Pendleton G. N., Paciesas W. S., Band D. L., 1998, ApJ, 506, L23
Protassov R., van Dyk D. A., Connors A., Kashyap V. L., Siemiginowska A., 2002, ApJ, 571, 545
Racusin J. et al., 2008, Nat, 455, 183
Racusin J. L., Cummings J., Holland S., Krimm H., Oates S. R., Page K., Siegel M., 2011, GCN Rep., 314
Rao A. R. et al., 2009, GCN Circ., 9665
Rao A. R. et al., 2011, ApJ, 728, 42
Roming P. W. A. et al., 2005, Space Sci. Rev., 120, 95
Rossi E., Lazzati D., Rees M. J., 2002, MNRAS, 332, 945
Rujopakarn W., Guver T., Pandey S. B., Yuan F., 2009, GCN Circ., 9515
Rumyantsev V., Pozanenko A., 2009, GCN Circ., 9539
Ryde F., 2004, ApJ, 614, 827
Ryde F., Pe'er A., 2009, ApJ, 702, 1211
Ryde F. et al., 2010, ApJ, 709, L172
Sakamoto T. et al., 2008, ApJS, 175, 179
Sakamoto T., Ukwatta T. N., Barthelmy S. D., 2009, GCN Circ., 9534
Salvaterra R. et al., 2009, Nat, 461, 1258
Sapir N., Katz B., Waxman E., 2011 (arXiv:1103.5075v1)
Sari R., Piran T., Halpern J. P., 1999, ApJ, 519, L17
Savchenko V., Neronov A., 2009, MNRAS, 396, 935
Schady P., 2009, GCN Circ., 9527

Schady P., Baumgartner W. H., Beardmore A. P., 2009a, GCN Rep., 232
Schady P. et al., 2009b, GCN Circ., 9512
Soderberg A. M. et al., 2008, Nat, 453, 469
Sparre M. et al., 2011, ApJ, 735, L24
Stanek K. Z. et al., 2003, ApJ, 591, L17
Starling R. L. C. et al., 2011, MNRAS, 411, 2792
Strüder L. et al., 2001, A&A, 365, L18
Tanvir N. R. et al., 2009, Nat, 461, 1254
Tavani M. et al., 2009, A&A, 502, 995
Thöne C. C., Guizy S., Castro-Tirado A., Gorosabel J., de Ugarte Postigo A., 2011a, GCN Circ., 11568
Thöne C. C. et al., 2011b, Nat, submitted (arXiv:1105.3015v2)
Tinney C., Stathakis R., Cannon R., Galama T., 1998, IAU Circ., 6896
Toma K., Ioka K., Sakamoto T., Nakamura T., 2007, ApJ, 659, 1420
Turner M. J. L. et al., 2001, A&A, 365, L27
Ukwatta T. N. et al., 2010, ApJ, 711, 1073
Updike A., Brittain S., Hartmann D., Colson A., Cumbee R., Hackett B., Lewis J., Kronberg M., 2009a, GCN Circ., 9529
Updike A., Brittain S., Hartmann D., Colson A., Cumbee R., Hackett B., Lewis J., Kronberg M., 2009b, GCN Circ., 9575
van Eerten H. J., Meliani Z., Wijers R. A. M. J., Keppens R., 2011, MNRAS, 410, 2016
von Kienlin A. et al., 2004, SPIE, 5488, 763
Vreeswijk P. M., Smette A., Malesani D., Fynbo J. P. U., Milvang-Jensen B., Jakobsson P., Jaunsen A. O., Ledoux C., 2008a, GCN Circ., 7444
Vreeswijk P. M., Milvang-Jensen B., Smette A., Malesani D., Fynbo J. P. U., Jakobsson P., Jaunsen A. O., Ledoux C., 2008b, GCN Circ., 7451
Waxman E., Mészáros P., Campana S., 2007, ApJ, 667, 351
Willingale R., Osborne J. P., O'Brien P. T., Ward M. J., Levan A., Page K. L., 2004, MNRAS, 349, 31
Woosley S. E., Bloom J. S., 2006, ARA&A, 44, 507
Xu D. et al., 2009, ApJ, 696, 971
Xue R. R., Fan Y.-Z., Wei D. M., 2009, A&A, 498, 671
Zeh A., Klose S., Hartmann D. H., 2004, ApJ, 609, 952
Zhang B., 2011, in Daigne F., Dubus G., eds, GRB studies in the SVOM era. Comptes Rendus Physique, 12, 206
Zhang B., Mészáros P., 2004, Int. J. Mod. Phys. A, 19, 2385
Zhang B., Fan Y. Z., Dyks J., Kobayashi S., Mészáros P., Burrows D. N., Nousek J. A., Gehrels N., 2006, ApJ, 642, 354
Zhang B.-B. et al., 2011, ApJ, 730, 141

This paper has been typeset from a TEX/LATEX file prepared by the author.